Impacts of Bond Type and Grafting Density on the Thermal, Structural and Transport Behaviors of Nanoparticle Organic Hybrid Materials-based Electrolytes

Tony G. Feric[a,c], Sara T. Hamilton[b,c], Md Ashraful Haque[d], Javad Jeddi[e], Joshua Sangoro[e], Mark D. Dadmun[d,f] and Ah-Hyung Alissa Park[a,b,c,*]

[a]Department of Chemical Engineering,
[b]Department of Earth and Environmental Engineering, and
[c]Lenfest Center for Sustainable Energy,
Columbia University, New York, NY 10027, USA
[d]Department of Chemistry
The University of Tennessee, Knoxville, TN, 37996, USA
[e]Department of Chemical and Biomolecular Engineering
The University of Tennessee, Knoxville, TN, 37996, USA
[f]Chemical Sciences Division
Oak Ridge National Laboratory, Oak Ridge, TN 37830, USA

Corresponding author: ap2622@columbia.edu

Keywords

Nanoparticle Organic Hybrid Materials (NOHMs), Electrolyte, Thermal stability, Viscosity, Conductivity, Hydrodynamic diameter, Redox Flow Batteries, CO_2 capture and conversion

Abstract

Nanoscale Organic Hybrid Materials (NOHMs) consist of a polymer tethered to a nanoparticle surface, and NOHMs formed with an ionic bond between the polymer and nanoparticle have been proposed for electrochemical applications. NOHMs exhibit negligible vapor pressure, chemical tunability, oxidative thermal stability and high ionic conductivity making them attractive in reactive and separation systems. In this study, NOHMs were synthesized by tethering Jeffamine M2070 (HPE) to SiO_2 nanocores via ionic (NOHM-I-HPE) and covalent (NOHM-C-HPE) bonding to investigate the effect of the bond type on the thermal, structural and transport properties of the tethered HPE. In the neat state, NOHM-C-HPE displayed the highest thermal stability in a nitrogen atmosphere, while NOHM-I-HPE was the most stable under oxidative conditions. Small angle neutron scattering (SANS) revealed the presence of multiple types of HPE polymers in aqueous solutions of NOHM-I-HPE (*i.e.,* tethered, interacting and free), whereas only tethered HPE was observed in NOHM-C-HPE systems. Moreover, the SANS profiles identified clustering of NOHM-C-HPE in aqueous solutions, but not in the corresponding NOHM-I-HPE solutions, suggesting that the free HPE chains stabilize the dispersion of NOHM-I-HPE. The results of this study elucidate how the bond type and grafting density can be used to tune the properties of NOHMs.

1. Introduction

In recent years, the costs associated with deploying renewable energy technologies have seen significant reductions though the feasibility of the large-scale transition to renewables remains limited by intermittency issues and a lack of reliable long-term energy storage solutions.[1,2] Thus, an emerging area of research involves the design and development of novel electrolyte materials for sustainable energy storage applications including the integrated capture and conversion of CO_2 and/or redox flow batteries (RFBs).[3–10] Currently, CO_2 conversion processes are limited by the solubility of CO_2 in the electrolyte phase (*i.e.,* only 34 mM)[11–13] and redox flow batteries are challenged by redox active species solubility and conductivity.[8,14,15] These challenges would affect the amount of CO_2 that can ultimately be converted and the total amount of energy that can be stored in the form of RFBs, thus highlighting the need for novel electrolyte design.

Ionic liquids,[4,6,16,17] deep eutectic solvents,[3,6,18–21] microemulsions,[22–26] and nanoparticle organic hybrid materials (NOHMs)[9,10,27–30] are currently being developed as novel electrolyte materials to improve the performance of various electrochemical systems. In particular, NOHMs consist of a polymer that is either ionically[31–38] or covalently tethered[31–33] to a nanoparticle core and possess a number of favorable properties including negligible vapor pressure,[31] oxidative thermal stability,[31,39–41] chemical tunability[9,42] and high ionic conductivity.[27,43] As a result, NOHMs have been extensively studied as water-lean CO_2 capture solvents and it has been shown that the organized structure of the polymer canopy in NOHMs leads to significantly less swelling compared to the untethered polymer, upon exposure to CO_2.[27,33,37,39,40,44–48] Moreover, the multitude of combinations of polymers[33], linkers[32,33] and nanoparticles[49] in NOHMs makes this class of materials especially desirable for applications such as integrated CO_2 capture and conversion systems[10,28] and redox flow batteries.[9,50] For example, the strategic selection of polymers with specific functional groups can optimize the binding energy for target species including small gaseous (*i.e.,* CO_2) or ionic species (*i.e.,* Cu^{+2}, Zn^{+2}). Though NOHMs synthesized with an ionic bond have been shown to be ionically conductive, they are challenged by high viscosity[31,34,51] and thus would need to be incorporated into electrolytes as additives. It has been shown that elucidating the transport[52–55] and structural[35,52,56] properties of electrolyte additives in solution is crucial to determining the overall electrochemical system performance.

In our recent work, we showed that in aqueous suspensions, the ionically grafted polymer chains in NOHM-I-HPE exist in different states (*i.e.,* tethered, interacting and free) where some possess stronger interactions with the SiO_2 nanoparticle surface than others.[34,35,51] Interestingly, the behaviors of the Jeffamine M2070 (referred to as HPE) canopy were found to be highly dependent on the concentration of NOHM-I-HPE,[35] solvent properties (*i.e.,* hydrogen bonding ability, polarity and molecular size)[34] and salt concentration.[51] For example, at higher concentrations of NOHM-I-HPE (*i.e.*, 40 wt.% loading in water), a significant amount of "free polymer" was observed in the aqueous solution that interacts with the grafted layer of the NOHM and alters the effective grafted layer thickness.[35] Furthermore, when NOHM-I-HPE was mixed with solvents with a significant number of hydrogen bond donating groups or high dielectric constant, the diffusion coefficient and NMR T_1 relaxation time of the polymer chains in NOHMs matched very closely to the untethered HPE polymer.[34] Lastly, the addition of $KHCO_3$ or NaCl to aqueous suspensions of NOHM-I-HPE was found to significantly reduce the solution viscosity,

suggesting that cations may compete with the HPE chains to occupy the hydroxyl surface sites on the nanoparticle surface and/or alter the conformation of the ionically grafted polymers.[35,51]

Because the dynamic exchange of the ionically tethered HPE canopy in NOHM-I-HPE was found to be highly dependent on the surrounding environment (*i.e.,* NOHMs concentration, solvent quality or salt concentration) and there exist three different types of HPE chains (*i.e.,* tethered, interacting and free) in NOHM-I-HPE, it remained unclear how the behaviors of covalently grafted HPE would compare. In this study, Jeffamine M2070 (HPE) was tethered to a 10 nm SiO_2 nanoparticle surface via ionic and covalent bond, at grafting densities of about 0.5 and 1.0 chains/nm^2, in order to determine the effect of the bond type on the resulting thermal, transport and structural properties of NOHMs. The materials, synthesized with different linker molecules, are referred to as NOHM-I-HPE and NOHM-C-HPE and are illustrated in **Figure 1A** and **Figure 1B**, respectively. The thermal stability of the NOHM-I-HPE and NOHM-C-HPE was tested in both non-oxidative (*i.e.,* nitrogen atmosphere) and oxidative (*i.e.,* air atmosphere) conditions to understand the performance of these materials under ideal and non-ideal conditions. Furthermore, an analysis of the transport properties (*i.e.*, viscosity and ionic conductivity) and small angle neutron scattering (SANS) profiles for the NOHM-I-HPE and NOHM-C-HPE dispersed in water revealed differences in the organization of the polymer canopy in response to an ionic stimulus (*i.e.,* 0.1 M $KHCO_3$). This is the first comprehensive study to report on comparable NOHM-based solutions and electrolytes with ionic and covalent bonds and investigate their structural and transport properties. The results from this study illustrate that NOHMs are exceptionally robust and stable materials, and their performance can easily be tuned for application as CO_2 capture materials or electrolyte additives.

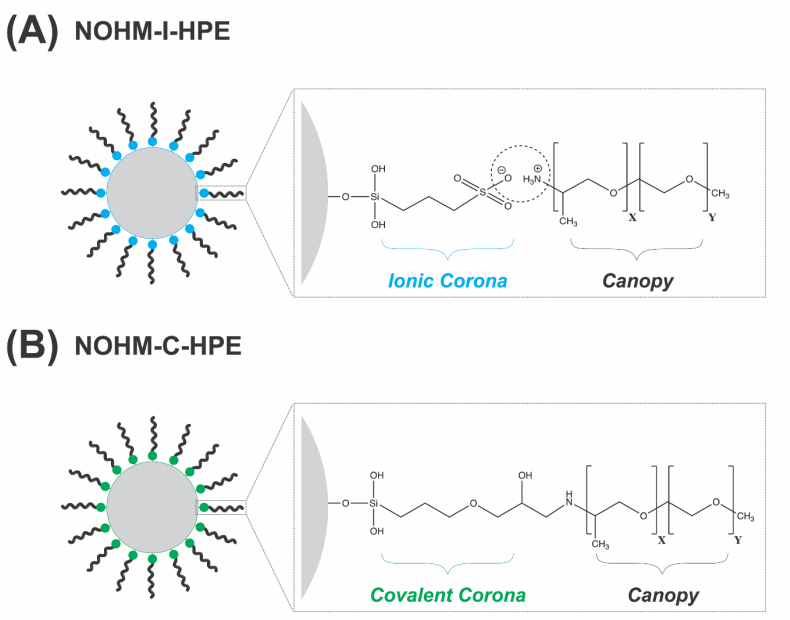

Figure 1. Structures of **(A)** NOHM-I-HPE and **(B)** NOHM-C-HPE used in this study. The number of poly(propyleneoxide) (X) and poly(ethyleneoxide) (Y) groups along the Jeffamine M2070 canopy are 10 and 31, respectively.

2. Results & Discussion

2.1 Effects of ionic vs. covalent bonding on HPE canopy phase transitions

To explore the effect of bond type on the mobility of the HPE chains, differential scanning calorimetry (DSC) was employed. Using a DSC instrument, the untethered HPE, SiO_2 nanoparticles, NOHM-I-HPE 0.8 (where the 0.8 refers to the grafting density of HPE in chains/nm^2) and NOHM-C-HPE 0.7 were heated and cooled between -100 and 100 °C at a scan rate of 2.5 °C/min, under an argon (Ar) atmosphere. From the heat flow data presented in **Figure 2**, the glass transition temperature (T_g), crystallization temperature (T_c), melting temperature (T_m) and polymer crystallinity (X_c) were determined and used to compare the HPE canopy mobility in these samples. The values are summarized in **Table 1**.

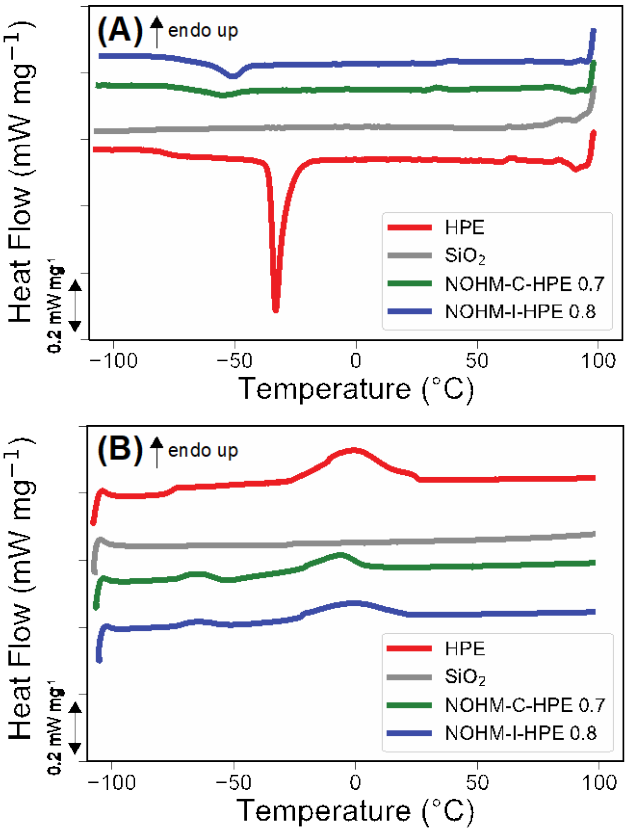

Figure 2. (A) Cooling and **(B)** heating DSC response for the untethered HPE, SiO_2 nanoparticles, NOHM-I-HPE 0.8 and NOHM-C-HPE 0.7 collected at 2.5 °C/min in argon atmosphere.

The nucleation density and growth are two factors that are known to control polymer crystallization.[41,57] Throughout the literature, the grafting of relatively short polymers to a nanoparticle surface has been shown to significantly affect the nucleation and crystal growth mechanisms due to polymer confinement.[40,46,57–59] From the cooling curves (See **Figure 2A**), it is immediately evident that the grafting of HPE to a nanoparticle surface *via* covalent or ionic bond significantly reduces the crystallinity of the canopy. The crystallization peak was very clearly defined in the case of the untethered HPE (63.5 ± 2.9 J/g), but became much subtler in the case of

NOHM-I-HPE 0.8 (7.7 ± 0.5 J/g) and NOHM-C-HPE 0.7 (4.0 ± 0.6 J/g). In addition, the crystallization temperature of the NOHMs was shifted by about 20-25 °C to lower temperatures, suggesting that the HPE confinement suppressed its crystallization, as has been reported in the literature.[41,57]

Table 1. Summary of thermal properties determined by the DSC analysis for HPE, NOHM-I-HPE 0.8 and NOHM-C-HPE 0.7, performed at a scan rate of 2.5 °C/min.

Property	***HPE***	***NOHM-I-HPE 0.8***	***NOHM-C-HPE 0.7***
Glass Transition Temperature, T_g	-75.9 ± 0.2 °C	-71.4 ± 0.1 °C	-70.9 ± 0.2 °C
Crystallization Temperature, T_c	-32.6 ± 0.4 °C	-51.6 ± 0.6 °C	-55.8 ± 1.5 °C
Melting Temperature, T_m	-1.1 ± 0.2 °C	-0.6 ± 0.2 °C	-6.4 ± 0.2 °C
Enthalpy of Crystallization, ΔH_c	63.5 ± 2.9 J/g	7.7 ± 0.5 J/g	4.0 ± 0.6 J/g
Enthalpy of Melting, ΔH_m	-66.4 ± 4.2 J/g	-19.6 ± 0.5 J/g	-11.7 ± 0.4 J/g
Polymer Percent Crystallinity, X_c	32.4 ± 2.1 %	9.5 ± 0.7 %	5.7 ± 0.2 %

Interestingly, the crystallization was further suppressed in NOHM-C-HPE 0.7 (-55.8 ± 1.5 °C) compared to NOHM-I-HPE 0.8 (-51.6 ± 0.6 °C). This suggests that the polymer is more mobile in the ionic NOHMs compared to covalent NOHMs. Due to the very low polymer loading in NOHM-I-HPE 0.4 and NOHM-C-HPE 0.5, phase transitions were not reliably detectable under the given conditions and thus are not depicted in **Figure 2**.

The T_g characterizes the transition of the polymer from a glass to a rubber in the heating direction and is widely used as a metric for assessing polymer mobility.[40,41,57,58] For example, the more mobile a polymer chain is, the lower the T_g.[40,41,57,58] Thus, for polymer grafted nanoparticles, it is expected to observe an increase in the glass transition temperature due to the reduced mobility associated with tethering the chains to the nanoparticle surfaces. From the heating curves displayed in **Figure 2B**, it was observed that the covalent and ionic tethering of HPE in NOHMs led to an increase in the glass transition temperature by about 4-5 °C compared to the untethered HPE. There were very subtle differences between the T_g of covalent and ionic NOHMs, though NOHM-C-HPE 0.7 displayed a slightly higher T_g than NOHM-I-HPE 0.8, which is consistent with the observed trend in crystallization behavior.

The melting temperature is known to be dependent on the thickness of the lamellae of the crystal structures. It is commonly reported for covalently grafted polymers to display a melting temperature that is lower than that of the untethered polymer. This has been described to result from the formation of thinner crystal structures due to crystal growth restrictions of the tethered polymer.[57] From the data presented in **Figure 2B**, it is apparent that the peak in the melting phase transition shifted to lower temperatures for NOHM-C-HPE 0.7 (-6.4 ± 0.2 °C) when compared to the untethered HPE canopy (-1.1 ± 0.2 °C). Interestingly, the melting temperature for NOHM-I-HPE 0.8 (-0.6 ± 0.2 °C) remained much closer to that of the untethered HPE canopy, indicating

that the thickness of the crystals in the ionically tethered polymer chains is likely similar to that of the untethered HPE.

Moreover, the polymer percent crystallinity was calculated for all samples using **Equation 5**. It was found that the in the NOHMs, the polymer percent crystallinity was significantly reduced compared to the untethered HPE canopy (32.4 ± 2.1 %), which agrees quite well with the literature for similar materials.[57] The polymer percent crystallinity for NOHM-I-HPE 0.8 (9.5 ± 0.7 %) was found to be slightly higher than that of the respective NOHM-C-HPE 0.7 (5.7 ± 0.2 %), further suggesting more facile crystal growth in the ionically grafted HPE chains than the covalently grafted ones. Overall, the analysis of the DSC data suggests that the HPE in NOHMs has a significantly reduced polymer mobility compared to the untethered HPE and the ionically tethered HPE chains are more mobile than the covalently tethered ones. The polymer mobility is an important parameter that governs how the HPE canopy in NOHMs will interact with and respond to its surrounding environment.

2.2 Impacts of bond type and graft density on non-oxidative and oxidative thermal stability of HPE canopy

For CO_2 capture and redox flow battery applications, a material's thermal and oxidative thermal stability are crucial to determining its robustness and long-term stability. In Direct Air Capture (DAC), for example, large concentrations of oxygen (21 vol.%) can cause materials to degrade quite rapidly, after just a few cycles.[60–64] Additionally, throughout the literature, there has been a lack of experimental data that explores the oxidative thermal stability of polymer grafted nanoparticles. Thus, we employed a thermogravimetric analyzer to determine the non-oxidative thermal (*i.e.,* nitrogen atmosphere) and oxidative thermal (*i.e.,* air atmosphere) degradation of the HPE polymer, NOHM-I-HPE and NOHM-C-HPE while heating from room temperature to 600 ºC, at a scan rate of 10 ºC/min. Additionally, we tested the HPE polymer functionalized with the ionic (SIT) and covalent (GPC) linkers under the same conditions and the thermal decomposition curves for all samples are displayed in **Figure 3**.

From **Figure 3A**, it is apparent that all the samples displayed a similar thermal stability in a nitrogen atmosphere, except NOHM-C-HPE 0.5 and NOHM-C-HPE 0.7, which were clearly distinct. The covalently grafted HPE chains had an onset of degradation shifted to higher temperatures, signifying an enhanced thermal stability, which is consistent with the literature for covalently grafted polymers.[57,65,66] It is important to note that in a nitrogen atmosphere, the ionically functionalized HPE, NOHM-I-HPE 0.4 and NOHM-I-HPE 0.8 displayed an onset of thermal degradation slightly earlier than the untethered HPE canopy. In our previous work, a kinetic thermal degradation analysis suggested that the ionic linker groups cause an autocatalytic degradation of the HPE canopy at elevated temperatures.[41] From the data presented in **Figure 3A**, it is evident that the covalent tethering of HPE to an SiO_2 nanoparticle enhances its thermal stability in a nitrogen atmosphere, while there is little to no improvement in the thermal stability of the same ionically tethered HPE. The thermal decomposition of the covalently functionalized HPE polymer (HPE + GPC) was very similar to that of the untethered HPE, thus highlighting how the heat shielding effect of the nanoparticle[66,67] and/or interfacial interactions[57] with the nanoparticle surface can lead to improvement of the thermal stability of polymers.

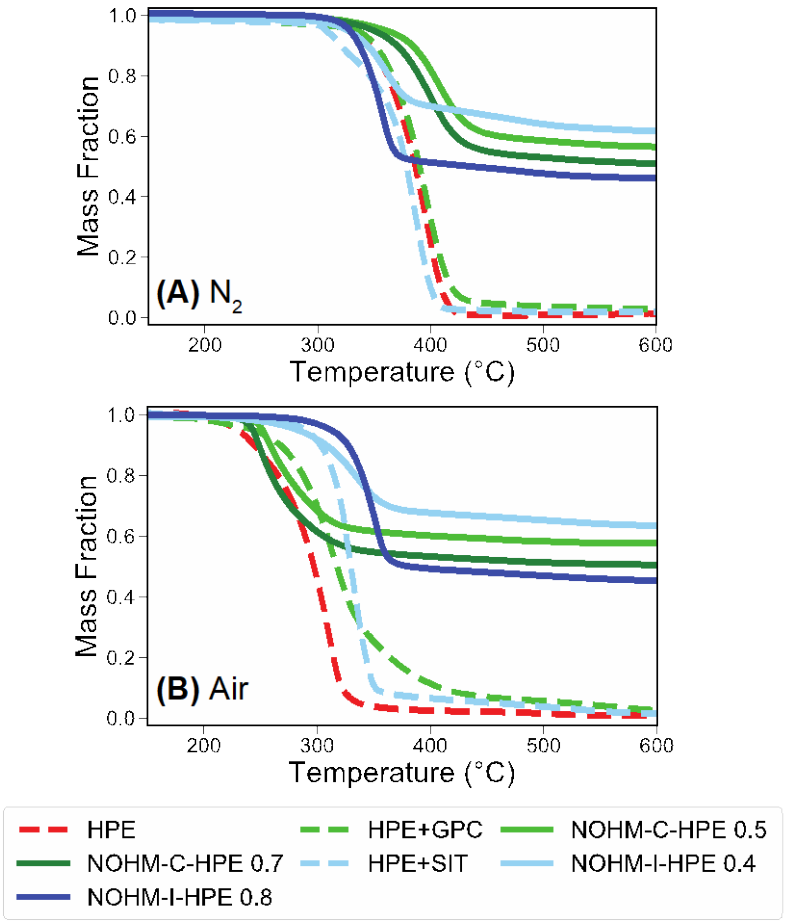

Figure 3. Thermogravimetric decomposition of the HPE, ionically and covalently functionalized HPE, NOHM-I-HPE and NOHM-C-HPE in **(A)** nitrogen or **(B)** air atmosphere, at a scan rate of 10 °C/min. The average of 3 trials is presented for each sample and the error was found to be within the thickness of the lines.

The data in **Figure 3B** indicate that the thermal stability of the NOHM-I-HPE samples and ionically functionalized HPE remained relatively unchanged when the atmosphere was changed from nitrogen to air. Conversely, the onset of thermal degradation for the untethered polymer, NOHM-C-HPE samples and covalently functionalized HPE was shifted significantly to lower temperatures upon exposure to an oxygen-containing atmosphere, thus highlighting their susceptibility to oxidative degradation. Many types of polymers have been shown to be sensitive to thermal degradation in the presence of oxygen.[39,41,64,68] These results suggest that the presence of oxygen has a significant impact on the degradation behaviors of covalently tethered polymers, while the ionically tethered polymers were much more resistant to oxidative degradation. In our previous work, we showed that the ionic tethering of the HPE canopy to SiO_2 nanoparticles in a higher grafting density and liquid-like NOHM-I-HPE lead to a significant enhancement in the oxidative thermal stability of HPE due to ionic bond stabilization of the N-terminus and a mass transfer limitation of oxygen.[39,41]

These differences in non-oxidative thermal and oxidative thermal stability of NOHM-I-HPE and NOHM-C-HPE suggest that bonding types and grafting density can be selected for

different applications. For example, NOHMs composed of an ionic bond and high grafting density could be useful in applications where large concentrations of oxidizing species (*i.e.,* Direct Air Capture at 21 vol% O_2) are present, whereas NOHMs composed of a covalent bond and low grafting density could be advantageous under high temperature and non-oxidizing conditions. As a result of this study, we recommend testing and reporting on the thermal stability of materials in both nitrogen and air atmospheres whenever possible.

These distinct thermal stabilities of NOHM-I-HPE and NOHM-C-HPE can be quantified by determining the $T_{10\%}$ in nitrogen and air atmospheres,[69] which in this case is defined as the temperature at which 10% of the initial organic content has been degraded in a non-isothermal degradation experiment. These values are summarized in **Table 2**. In a nitrogen atmosphere, the $T_{10\%}$ values are slightly higher in the case of NOHM-C-HPE 0.5 and NOHM-C-HPE 0.7, while in an air atmosphere, the $T_{10\%}$ values are significantly higher for NOHM-I-HPE 0.4 and NOHM-I-HPE 0.8. The thermal stability for all samples is clearly higher in a nitrogen atmosphere than it is in an air atmosphere because polymers are known to undergo oxidative degradation in addition to thermal degradation.[41,68] Furthermore, the difference between the $T_{10\%}$ in nitrogen and the $T_{10\%}$ in air atmospheres, defined as, $\Delta T_{10\%}$ (N_2 - Air), can serve as metric to quantify the susceptibility of a material to oxidative thermal degradation. Based on this analysis, it is evident that the onset of thermal degradation is reduced by about 100 °C when the atmosphere is switched from nitrogen to air for HPE, NOHM-C-HPE 0.5 and NOHM-C-HPE 0.7. However, this difference is much less pronounced in NOHM-I-HPE 0.4 (48 ± 2 °C) and especially NOHM-I-HPE 0.8 (15 ± 2 °C). Overall, these results suggest that the ionic tethering of the HPE canopy to an SiO_2 nanoparticle surface significantly improves its resistance to oxidative thermal degradation, while covalent tethering provides little to no enhancement of polymer stability. Thus, NOHMs composed of an ionic bond would be great candidates for CO_2 capture applications where concentrations of oxidizing species are high (*i.e.,* Direct Air Capture).

Table 2. $T_{10\%}$ for the degradation of all samples in nitrogen and air at a scan rate of 10 °C/min and the difference between the $T_{10\%}$ in nitrogen and $T_{10\%}$ in air ($\Delta T_{10\%}$ (N_2 - Air)) is also calculated and reported.

	HPE	***NOHM-I-HPE 0.4***	***NOHM-I-HPE 0.8***	***NOHM-C-HPE 0.5***	***NOHM-C-HPE 0.7***
N_2	346 ± 5 °C	320 ± 1 °C	329 ± 1 °C	355 ± 1 °C	349 ± 1 °C
Air	244 ± 4 °C	272 ± 1 °C	314 ± 1 °C	250 ± 1 °C	243 ± 1 °C
$\Delta T_{10\%}$ (N_2 - Air)	102 ± 6 °C	48 ± 2 °C	15 ± 2 °C	105 ± 2 °C	106 ± 2 °C

In order to directly compare the thermal degradation behaviors of the HPE chains in untethered HPE, NOHM-I-HPE and NOHM-C-HPE in both non-oxidative and oxidative conditions, the weight loss was converted to a dimensionless extent of conversion parameter, α. The extent of conversion (α) is commonly used in kinetic thermal degradation analyses because of its ability to normalize for the mass of any inert species present (*i.e.,* the SiO_2 nanoparticles). The extent of conversion, α, can be determined at a given temperature (T) or reaction time (t) by

$$\alpha = \frac{w_i - w}{w_i - w_f} \qquad \textbf{Eq. (1)}$$

where w_i is the initial weight fraction of the sample, w is the weight fraction of the sample at a given time (t) or temperature (T) and w_f is the weight fraction of the sample at the end of the thermal decomposition.[70,71] By comparing the degradation in terms of this dimensionless parameter, α, the details of the onset of HPE degradation in free HPE, NOHM-I-HPE and NOHM-C-HPE can be more clearly identified. It should be noted, however, that this method does not normalize for the presence of the linker molecules in the functionalized polymer and NOHMs samples.

Figure 4 presents α and its derivative with respect to temperature ($d\alpha/dT$) for HPE, NOHM-I-HPE and NOHM-C-HPE in nitrogen (100% N_2) and air (79% N_2, 21% O_2) atmospheres. By comparing α as a function of temperature (See **Figure 4-A1** and **4-A2**), the trends discussed in the previous paragraphs are confirmed. More specifically, it can be observed that in a nitrogen atmosphere, for both ionically and covalently grafted HPE chains, the lower the grafting density the more stable the resulting material (*i.e.,* a higher temperature is required to reach the same α). This has been previously reported to result from a heat shielding effect of the nanoparticle[66,67] and a greater number of polymer-nanoparticle interaction sites at lower grafting densities.[57] For example, at lower grafting densities, there is more physical space for the polymer to occupy on the nanoparticle surface, thus leading to an increase in the extent and strength of interactions between the polymer chains and nanoparticles.

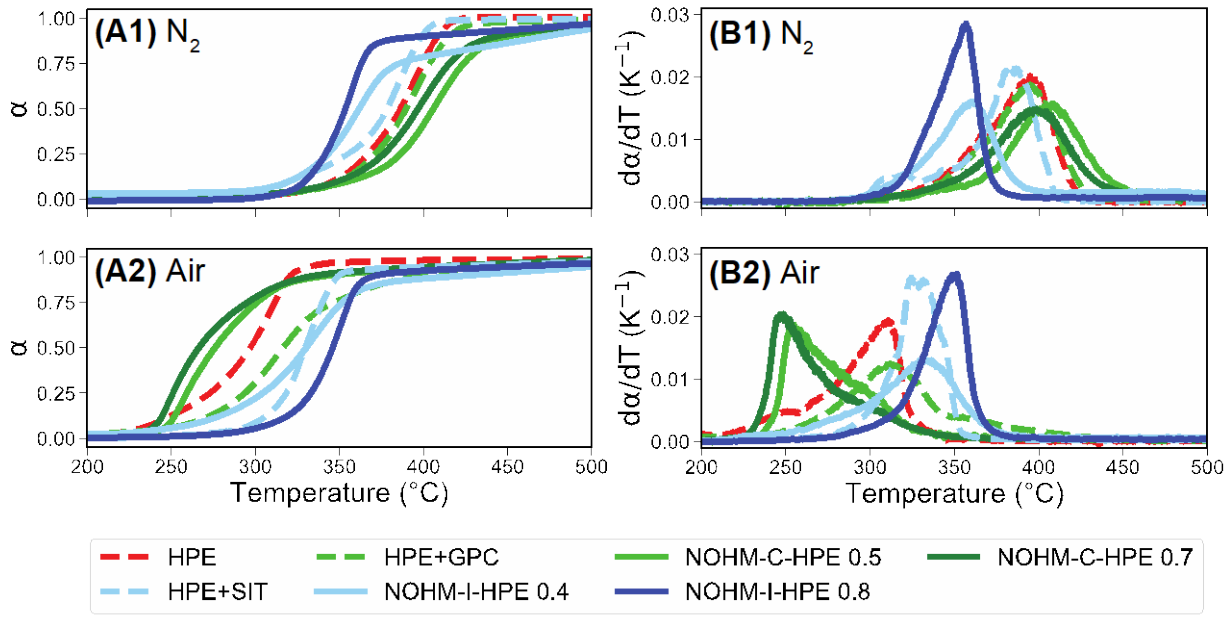

Figure 4. Effect of temperature on the extent of conversion (α) of all samples in **(A1)** nitrogen or **(A2)** air atmosphere. The corresponding derivatives with respect to temperature ($d\alpha/dT$) are shown in **(B1)** nitrogen and **(B2)** air environments**.**

In an oxygen-containing atmosphere (*i.e.,* air), the same trend is observed for the NOHMs composed of a covalent bond, where NOHM-C-HPE 0.5 demonstrated a slightly improved stability compared to NOHM-C-HPE 0.7. However, in the case of the ionically tethered HPE

canopy, NOHM-I-HPE 0.8 displayed a higher oxidative thermal stability than NOHM-I-HPE 0.4. Similar to our previous work, this is attributed to limited mass-transfer of oxygen in the gel-like structure of NOHM-I-HPE 0.8 (See **Table 3**).[41] At this higher grafting density, the behavior of the material resembles that of a very viscous liquid, while NOHM-I-HPE 0.4 is a solid film (See **Table 3**). Thus, the significant enhancement of oxidative thermal stability arises from a combination of ionic bond stabilization of the HPE N-terminus and oxygen mass transfer resistance, as we recently reported for a higher grafting density liquid-like NOHM-I-HPE.[41]

By comparing the data in **Figure 4-B1** and **4-B2**, the trends reported in **Table 2** can be visually observed by examining how the maximum in ($d\alpha/dT$) shifts when the atmosphere is changed from nitrogen to air. The peak in ($d\alpha/dT$) shifts by roughly 100 °C for HPE, NOHM-C-HPE 0.5 and NOHM-C-HPE 0.7, while there is only a minor shift in the ($d\alpha/dT$) peak of NOHM-I-HPE 0.4. Interestingly, there is almost no change in the ($d\alpha/dT$) peak of NOHM-I-HPE 0.8, thus highlighting the potential for NOHMs composed of an ionic bond to be used in applications that involve elevated temperatures and harsh oxidizing conditions.

2.3 Hydrodynamic diameter of NOHMs in dilute solution as a function of bond type and HPE grafting density

In addition to thermal stability, it is important to investigate the behaviors of NOHMs in the solution phase in order to design them for electrochemical applications, including CO_2 conversion and redox flow batteries. The structure and transport properties of other novel electrolyte materials such as ionic liquids and deep eutectic solvents have been found to play a role in determining the overall system performance.[52–56] To further examine the effects of bond type and grafting density on the resulting hydrodynamic size of NOHMs in aqueous suspension, dynamic light scattering (DLS) was employed. **Figure 5A** shows a representative population distribution for the hydrodynamic diameter (d_H) of HPE, SiO_2 nanoparticles, NOHM-I-HPE 0.4, NOHM-I-HPE 0.8, NOHM-C-HPE 0.5 and NOHM-C-HPE 0.7 at 0.1 wt.% and 25 °C. In **Figure 5B**, the average hydrodynamic diameter of five trials is presented for all samples and the values obtained here matched closely to what has previously been reported in the literature for similar NOHMs materials.[72] Taken together, the data in **Figure 5A** and **5B** depict that the hydrodynamic diameter of the NOHM-C-HPE was slightly larger than that of the corresponding NOHM-I-HPE.

In order to directly compare the extent of polymer stretching and/or collapse in the NOHMs composed of ionic and covalent bond, the thickness of the NOHMs' polymer canopy (d_N) was determined by the following equation:

$$d_N = \frac{d_{NOHMs} - d_{NP}}{2} \qquad \textbf{Eq. (2)}$$

where d_{NOHMs} is the measured hydrodynamic diameter of NOHMs (ionic or covalent) and d_{NP} is the measured hydrodynamic diameter of the SiO_2 nanoparticles (d_{NP} = 10.6 ± 0.9 nm) in water at a concentration of 0.1 wt.%. It is of importance to note that this method assumed that the SiO_2 particle was perfectly smooth and that the tethered polymer displayed a conformation that was uniform around the SiO_2 nanoparticle. To compare the relative stretching of the polymer canopy in NOHMs to the untethered HPE, **Figure 5C** displays the ratio of the thickness of the NOHMs polymer canopy (d_N) to the measured hydrodynamic diameter of the HPE chains (d_P = 1.66 ± 0.12 nm). It is evident that the covalently tethered polymers in NOHM-C-HPE displayed a slight increase in the amount of polymer stretching compared to the ionically tethered polymers in the

corresponding NOHM-I-HPE samples, though the differences are very subtle. The increased grafting density also increased the hydrodynamic diameter since the polymers experience reduced mobility when tethered to the nanoparticle surface, but again, the difference was not large. This suggests that the hydrodynamic diameter of NOHMs in a dilute aqueous suspension (*i.e.*, 0.1 wt.%) is only weakly dependent on the bond type used to tether the polymer to the nanoparticle surface and the grafting density.

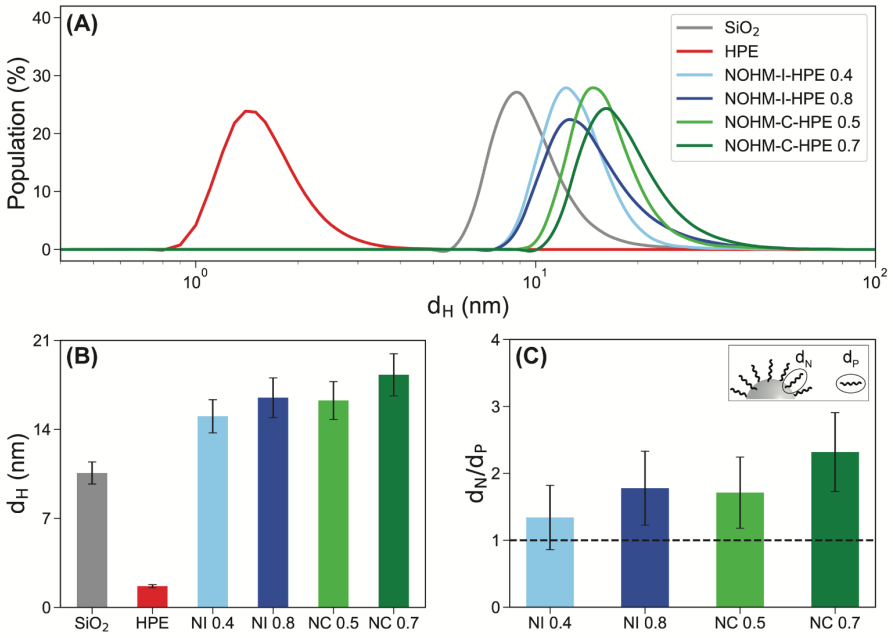

Figure 5. (A) Representative hydrodynamic size populations of HPE, SiO_2 nanoparticles, NOHM-I-HPE and NOHM-C-HPE, measured at a concentration of 0.1 wt.% and 25 °C. **(B)** Average hydrodynamic size is reported after 5 measurements. **(C)** Normalized hydrodynamic diameter of the ionically or covalently tethered HPE canopy in NOHM-I-HPE or NOHM-C-HPE (d_N) by that of the untethered HPE (d_P).

2.4 Elucidation of the structure of ionically and covalently grafted HPE of NOHMs in aqueous solutions and electrolytes

Our earlier studies have shown that the polymers in NOHM-based fluids often exist in multiple states such as tethered, interacting and free HPE chains.[34,35,51] Those earlier studies were only focused on NOHM-I-HPE, and we anticipated that NOHM-C-HPE would lead to different binding interactions in the solution phase, with and without salts. Thus, small-angle neutron scattering (SANS) experiments were completed to identify the effect of the bond type on the structure and organization of the polymer and nanoparticles in NOHM-based fluids and electrolytes. **Figure S3** shows the SANS profiles of the 1 wt.% and 3 wt.% NOHM-I-HPE 0.8 with and without the presence of 0.1 M $KHCO_3$ in the solution. A previous study on similar aqueous solutions of 10-40 wt.% NOHM-I-HPE, with a grafting density 2-2.5 chain/nm^2 (significantly higher than those of this study), showed that the scattering intensity decreases at low-Q and increases at high-Q with NOHM loading, which was indicative of the presence of free polymer in the solution.[35]

However, at 1 wt.% and 3 wt.% loading of NOHM-I-HPE 0.8, we did not observe such a phenomenon. Therefore, initially, only the core-shell model was used to fit the scattering profile. During the fitting process, it was realized that including only the core-shell sphere model does not capture the high-Q region of both the 1 wt.% and 3 wt.% NOHM-I-HPE 0.8 scattering profiles (See **Figure S4**). In our previous study, we observed that the high-Q region of the scattering profile is correlated to the presence of free polymer in the NOHM-I-HPE solution. Therefore, failure to capture the high-Q region of the 1 wt.% and 3 wt.% NOHM-I-HPE 0.8 scattering profiles indicated that there was free polymer in the solution that was not grafted to the nanoparticle and ultimately, the combined model of core-shell sphere and polymer excluded volume was able to successfully fit the NOHM-I-HPE 0.8 SANS profiles (See **Figure S4**).

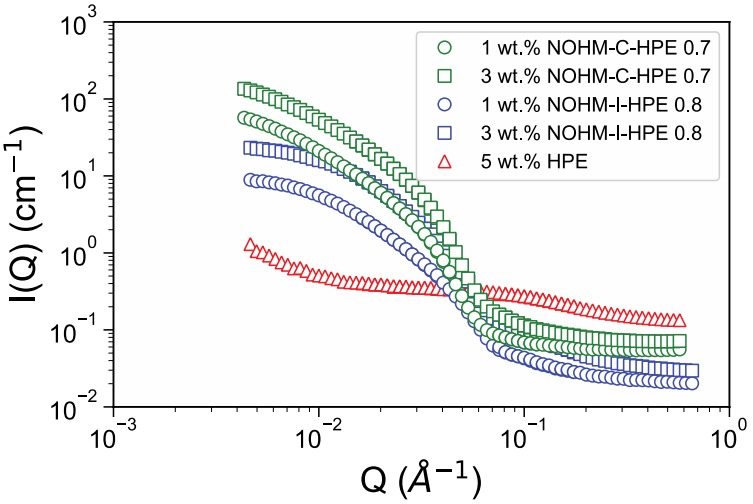

Figure 6. Small-angle neutron scattering profiles for 1 wt.% (circles) and 3 wt.% (squares) NOHM-C-HPE (green) and NOHM-I-HPE 0.8 (blue) in water. The scattering profile of 5 wt.% HPE is also included (red triangles). The samples presented are not doped with any salt.

Figure 6 shows $I(Q)$ plotted as a function of Q for both the NOHM-C-HPE 0.7 and NOHM-I-HPE 0.8, at concentrations of 1 wt.% and 3 wt.%, in the absence of salt. It is immediately evident that the intensity of the NOHM-C-HPE scattering profile is significantly higher compared to that of the NOHM-I-HPE. This is ascribed to the presence of clusters of NOHMs in the solution. Therefore, a fractal core-shell model was used to model the scattering, which was able to capture the detailed structure of the fractal aggregate and the thickness of the grafted polymer in the NOHM-C-HPE samples. However, the fractal core-shell model alone was not able to capture the measured scattering across a portion of the Q range (0.08 Å^{-1} < Q < 0.1 Å^{-1}). This Q range monitors structure on the length scale of ~62 Å-78 Å, and thus this deviation is consistent with the presence of dispersed individual NOHM-C-HPE particles. Therefore, a combined fractal core-shell and core-shell sphere model was applied to fit both the 1 wt.% and 3 wt.% NOHM-C-HPE 0.7 solutions with and without salt over the entire Q range (See **Figure S3** and **Figure S5**). The fitting shows that the fractal aggregate has a fractal dimension of ~2.5 and a correlation length of 150-170Å in the NOHM-C-HPE 0.7 solutions. To estimate the size of the fractal aggregates, the Guinier model[73] is used to fit the low-Q region (0.004 Å^{-1} < q < 0.01 Å^{-1}) of the scattering profile. The Guinier model fit indicated that the radius of gyration (R_g) of the clusters is ~200 Å (*i.e.,* 20 nm).

The application of these combined models provides a measure of the thickness of the polymer layer grafted to the silica nanoparticle of NOHM-I-HPE 0.8 and NOHM-C-HPE 0.7, in the presence or absence of supporting electrolyte, where the results are displayed in **Figure 7**. Careful analysis of the data indicates that there is a nominal decrease in the thickness of the shell with increasing NOHM loading. This result is consistent with our previous study,[35] where we observed that the interaction of the free polymer with the grafted layer alters the effective thickness of the grafted layer. Moreover, the data indicate that the grafted layer thickness of NOHM-C-HPE is larger than the grafted layer of NOHM-I-HPE. In agreement with our previous work, the addition of 0.1 M $KHCO_3$ to a suspension of NOHM-I-HPE was found to significantly reduce the effective thickness of the grafted layer.[35] Conversely, the decrease in thickness of the grafted layer of NOHM-C-HPE compared to NOHM-I-HPE with addition of salt is nominal, suggesting that salt has little to no effect on HPE polymer if it is covalently bonded to silica nanoparticles.

To understand the difference in thickness of the grafted layer between NOHM-C-HPE and NOHM-I-HPE, we investigated the size (radius of gyration, R_g) of the HPE polymer in aqueous solution (See **Figure 6**). The SANS scattering profile of HPE in aqueous solution was fit to a polymer excluded volume model that shows that the R_g of the polymer is 12 Å, which is consistent with the DLS results presented in the previous section. Now, comparing the size of the free HPE polymer to that of the grafted layer (corona + canopy) thickness of both NOHM-I-HPE and NOHM-C-HPE clearly indicates that the presence of polymer not grafted to the nanoparticle surface in NOHM-I-HPE solution alters the *effective* thickness of the grafted layer. Conversely, the grafted layer thickness of NOHM-C-HPE is the apparent thickness of the grafted layer because there is no free polymer in the solution.

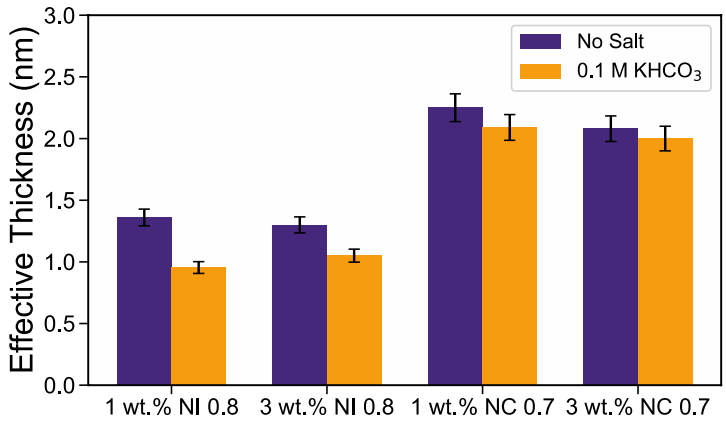

Figure 7. Change in the effective thickness of the grafted layer upon salt addition (0.1 M $KHCO_3$) for NOHM-I-HPE 0.8 and NOHM-C-HPE 0.7.

The overall SANS analysis of NOHM-I-HPE and NOHM-C-HPE indicates that the presence or absence of free polymer appears to drive the formation of an aggregated NOHM assembly or a well dispersed NOHM assembly. This realization correlates well with a study done by McDonald *et al.*, where it was found that the presence of excess HPE polymer added to a similar NOHM-C-HPE system stabilized the NOHM particles and allowed the formation of a well-dispersed NOHM assembly in the liquid polymer nanocomposite.[72]

2.5 Distinct transport behaviors of NOHM-based solutions and electrolytes with varied bond types and HPE grafting density

The transport properties of electrolytes ultimately affect mass transfer and kinetics which are crucial to the design of any electrochemical system. To understand how the bond type and graft density affect the transport properties, we measured the viscosity of HPE, the bare SiO_2 nanoparticles, NOHM-I-HPE and NOHM-C-HPE at concentrations ranging from 0-10 wt.%, in the absence and presence of 0.1 M $KHCO_3$. This concentration of salt was selected because this was recently found to be near the experimentally observed transition from the ionic stimuli responsive regime to the saturation regime of a higher grafting density liquid-like NOHM-I-HPE.[51] The specific viscosity is a dimensionless measure of the viscosity and was used in this case to directly compare the effect of polymer, nanoparticle or NOHMs addition to the overall solution viscosity. The specific viscosity (η_{sp}) can be determined by

$$\eta_{sp} = \frac{\eta - \eta_s}{\eta_s} \quad \textbf{Eq. (3)}$$

where η is the viscosity of the solution/electrolyte containing polymer, nanoparticles or NOHMs and η_s is the viscosity of the solvent (*i.e.,* water or 0.1 M $KHCO_3$).

The data in **Figure 8A** agree with the DLS and SANS data presented in the previous sections, as NOHM-C-HPE 0.5 and NOHM-C-HPE 0.7 were slightly more viscous than NOHM-I-HPE 0.4 and NOHM-I-HPE 0.8. This can primarily be explained by the larger hydrodynamic diameter and larger effective thickness of the covalently tethered polymers by the DLS measurements and SANS analysis. Additionally, viscosity was found to increase with grafting density, likely due to polymer chain stretching increasing the effective hydrodynamic volume.

Both types of NOHMs were more viscous than the untethered HPE. However, it should be noted that the specific viscosity of the SiO_2 nanoparticles is consistently below that of the HPE in **Figure 8A** due to the much higher density of SiO_2 (2.65 g/cm^3) compared to that of the untethered HPE (1.07 g/cm^3). When presented as a function of the volume fraction, the specific viscosity of the ~10 nm SiO_2 nanoparticles was in fact larger than that of the ~2 nm untethered HPE chains (See **Figure S6**), as viscosity usually increases with hydrodynamic diameter. To keep consistent with the polymer literature, we employed the convention of presenting the concentration in terms of the mass per unit volume.

By comparing the data presented in **Figure 8A** and **8B**, we observe a reduction in the specific viscosity of NOHM-I-HPE and NOHM-C-HPE after the addition of 0.1 M $KHCO_3$, though the decrease is much more pronounced for NOHM-I-HPE. After the addition of 0.1 M $KHCO_3$, solutions containing NOHM-I-HPE 0.4 and NOHM-I-HPE 0.8 became even less viscous than the corresponding untethered polymer solutions. To quantitatively assess the change in viscosity induced by the addition of 0.1 M $KHCO_3$, the relative percentage difference in the viscosity before and after salt addition ($\Delta\eta$), was calculated and plotted in **Figure 9** as a function of the polymer, nanoparticle or NOHMs concentration. The relative percentage difference in the viscosity before and after 0.1 M $KHCO_3$ addition ($\Delta\eta$) can be calculated by the following

$$\Delta\eta = \frac{\eta_{SE} - \eta}{\eta} \times 100\% \quad \textbf{Eq. (4)}$$

where η is the viscosity of the aqueous solution, *i.e.,* before salt addition, and η_{SE} is the viscosity of the electrolyte solution, *i.e.,* after supporting electrolyte (SE) addition.

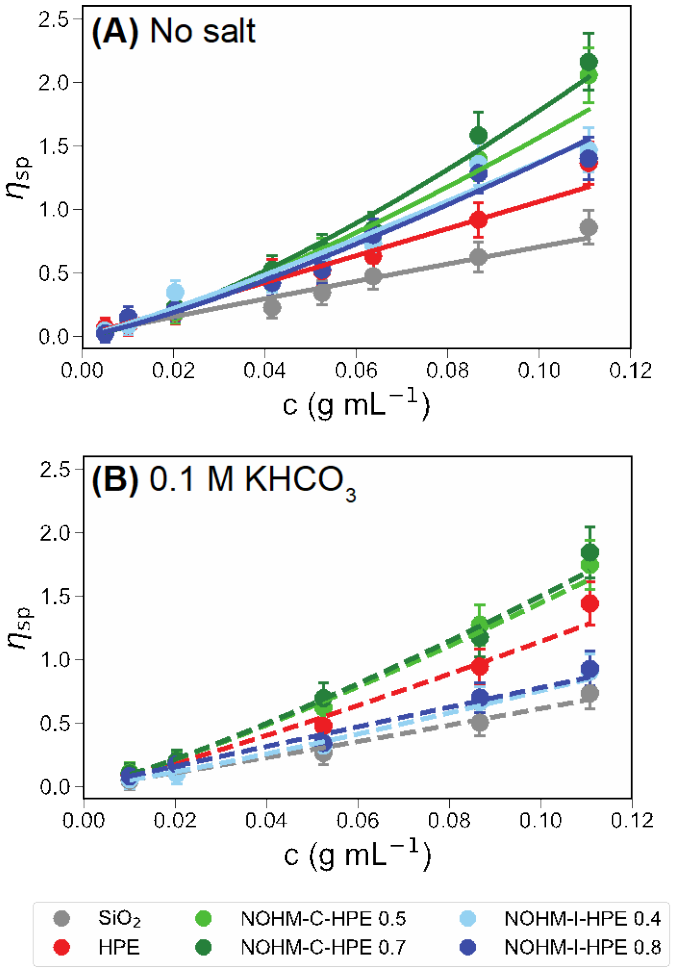

Figure 8. Specific viscosity plotted as a function of the concentration for HPE, SiO_2, NOHM-I-HPE and NOHM-C-HPE in the **(A)** absence and **(B)** presence of 0.1 M $KHCO_3$. Power law fittings have been applied to the data to guide the eye.

Across the polymer/nanoparticle/NOHMs concentration range studied (0-10 wt.%), it is apparent that the change in viscosity remained less than ± 5% for the HPE, suggesting that the addition of 0.1 M $KHCO_3$ does not significantly affect the mobility of the untethered HPE chains.[35,51] Upon the addition of 0.1 M $KHCO_3$, the SiO_2 nanoparticles, NOHM-C-HPE 0.5 and NOHM-C-HPE 0.7 showed a slight reduction in viscosity compared to the untethered HPE. This can be explained by K^+ ions screening out some of the nanoparticle-nanoparticle interactions, which has been similarly shown to lead to a smaller hydrodynamic size of bare nanoparticles.[74,75] In the case of the covalent NOHMs, a slight collapse of the polymer chains in response to ionic stimulus was observed based on the SANS analysis in the previous section and has also been observed for similarly grafted polymer chains.[76,77] Charge screening or polymer collapse would lead to a slightly reduced apparent hydrodynamic size of the NOHMs, which would be expected to lead to a reduced viscosity.[28,78,79]

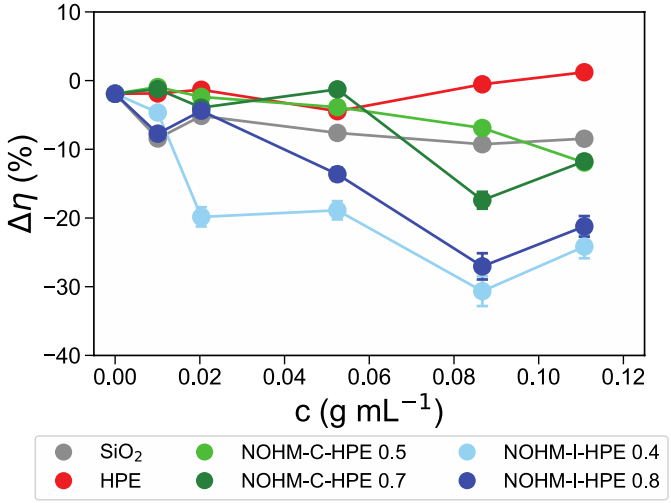

Figure 9. Percent difference in viscosity upon the addition of 0.1 M $KHCO_3$ depicted as a function of the concentration of HPE, SiO_2, NOHM-I-HPE and NOHM-C-HPE.

Interestingly, at concentrations greater than or equal to 5 wt.%, the salt addition caused a significant reduction in the viscosity of NOHM-I-HPE 0.4 and NOHM-I-HPE 0.8 compared to all other samples. Above a concentration of 5 wt.%, the decrease in viscosity was around 30%, which is about 2-3 times greater than what was observed for Δη of the bare SiO_2 nanoparticles or NOHM-C-HPE 0.5 and NOHM-C-HPE 0.7. Thus, the reduction in the viscosity of NOHM-I-HPE cannot be explained by an ionic screening of the exposed nanoparticle surface charge or polymer shrinking alone. In combination with the SANS analysis, these results suggest that the addition of 0.1 M $KHCO_3$ also affected the ionic tethering of the HPE to the SiO_2 nanoparticle. For example, the addition of K^+ ions may compete with the polymer chains for the nanoparticle active sites, thus causing them to be released into the bulk solution where they are much more mobile. For both the NOHM-I-HPE and NOHM-C-HPE, grafting density did not appear to cause major differences in the viscosity change in response to salt addition.

To complement the viscosity data, we also measured the ionic conductivity of HPE, the bare SiO_2 nanoparticles, NOHM-I-HPE and NOHM-C-HPE at concentrations ranging from 1-10 wt.%, in the absence and presence of 0.1 M $KHCO_3$. In **Figure 10A**, it can be observed that the SiO_2 nanoparticles were about an order of magnitude more conductive than untethered HPE or the NOHMs. Solutions containing NOHM-I-HPE 0.4 or NOHM-I-HPE 0.8 were about 2-3 times more conductive than the corresponding solutions of untethered HPE, NOHM-C-HPE 0.5 or NOHM-C-HPE 0.7. This can be explained by a combination of the conductive nature of the ionic bond linking the HPE chains to the SiO_2 nanoparticles and the exposed SiO_2 surface sites. The slight improvement in conductivity of NOHM-C-HPE 0.5 relative to the untethered HPE polymer is likely due to the presence of exposed surface charge on SiO_2 surface sites not used for polymer tethering.

In terms of the grafting density, the covalent NOHMs displayed the expected trend, *i.e.*, conductivity should decrease with grafting density because more of the SiO_2 surface sites are blocked by the tethered HPE at the surface. In the ionic NOHMs, we saw the opposite trend where NOHM-I-HPE 0.8 was more conductive than NOHM-I-HPE 0.4. This results from the additional linker groups that were added to the SiO_2 nanoparticles in order to increase the grafting density of

the HPE. Since the grafting process is not 100% efficient and untethered HPE chains were removed during the dialysis procedure, the additional exposed linker groups would be expected to increase the conductivity in NOHM-I-HPE 0.8 (See Experimental Section).

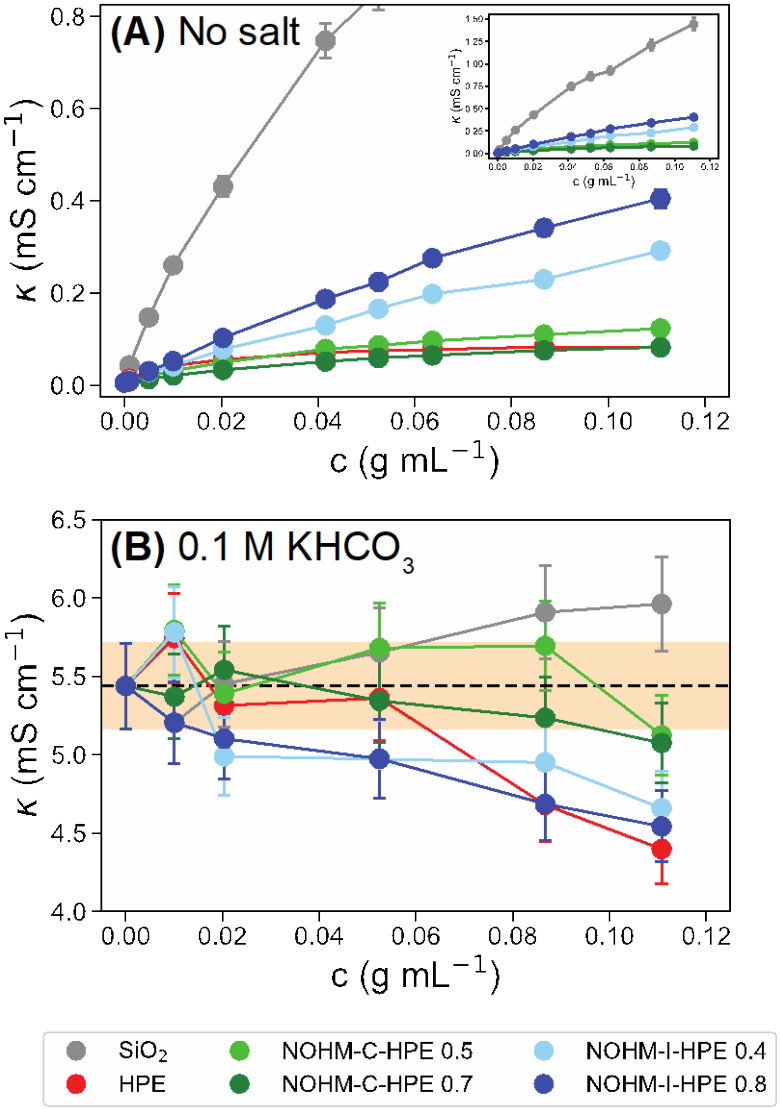

Figure 10. Conductivity depicted as a function of the concentration for HPE, SiO_2, NOHM-I-HPE and NOHM-C-HPE in the **(A)** absence and **(B)** presence of 0.1 M $KHCO_3$.

Figure 10B illustrates the dependence of ionic conductivity on the concentration of HPE, SiO_2, NOHM-I-HPE and NOHM-C-HPE, in the presence of 0.1 M $KHCO_3$. When compared to **Figure 10A**, the conductivity was significantly increased due to the presence of a conductive supporting electrolyte. The dotted black line in this figure denotes the conductivity of 0.1 M $KHCO_3$ and the yellow shaded region represents the ± 5% error window. From this data, it is clear that as the HPE concentration in solution increases, the conductivity steadily decreases. The amine terminus of the Jeffamine M2070 polymer is likely protonated in aqueous solution. Upon the addition of salt, the protonated amine end (NH_3^+) could interact with some of the HCO_3^- anions in

solution, leading to a slight neutralization of the charge and an apparent reduction in the conductivity. Similarly, the ether groups could interact with some of the K^+ cations, as has been shown in the literature.[80,81]

In the presence of 0.1 M $KHCO_3$, the conductivity of all solutions was dominated by the presence of supporting electrolyte. However, there were still distinct differences between NOHM-I-HPE and NOHM-C-HPE systems. The bare SiO_2 nanoparticles displayed a slight increase with concentration, likely due to the significant increase in charged species in the solution. The conductivity of NOHM-C-HPE 0.5 and NOHM-C-HPE 0.7, in the presence of 0.1 M $KHCO_3$, remained quite constant as a function of NOHMs concentration, though a slight decrease was observed at higher NOHMs loadings. This suggests that the covalent bond linking the HPE canopy to the nanoparticle was not affected by the presence of an ionic stimulus and the main interactions between the $KHCO_3$ and NOHMs was through the ether groups on the HPE canopy.

Conversely, the conductivity trends for NOHM-I-HPE 0.4 and 0.8 appear to follow closely to that of the untethered HPE, suggesting that the addition of 0.1 M $KHCO_3$ may disrupt the ionic bond that links the polymer to the nanoparticle surface by neutralizing the amine terminal group. This trend agrees well with the significant reduction in the viscosity of the ionic NOHMs upon the addition of ionic stimulus (See **Figure 8 and 9**) and the results of the SANS analysis presented in the previous section.

3. Conclusions

The results of this study clearly indicate that the nature of the bond (*i.e.,* ionic vs. covalent) that links the HPE canopy to the SiO_2 nanoparticle surface leads to significant differences in the thermal, structural and transport properties of NOHMs. In terms of thermal stability, the covalently tethered HPE canopy in NOHM-C-HPE showed the highest stability in a nitrogen atmosphere and this finding is consistent with the literature.[57,65,66] However, the covalent NOHMs did not show an improvement to the thermal stability of the HPE canopy in the presence of air. Interestingly, NOHM-I-HPE 0.8 displayed the highest oxidative thermal stability compared to all other materials studied in this work, thus making NOHMs synthesized with an ionic bond and higher grafting density especially interesting for CO_2 capture applications where larger amounts of oxygen may be present (*i.e.,* Direct Air Capture).[60–64] Our recent work has shown that the enhanced oxidative thermal stability of liquid-like NOHM-I-HPE arises from an ionic bond stabilization of the N-terminus of the HPE polymer and a mass transfer resistance to oxygen as a result of an orders of magnitude increase in the viscosity of liquid-like NOHMs compared to the untethered polymer.[41] Furthermore, the analysis of SANS profiles and the measurement of viscosity and conductivity elucidated significant differences between covalently and ionically grafted polymers. For example, clustering was observed in solutions containing NOHM-C-HPE, but not in those containing NOHM-I-HPE, suggesting that the presence of free and/or interacting polymers in the NOHM-I-HPE solutions may stabilize their dispersion. In agreement with the calculated effective grafted layer thickness, the addition of 0.1 M $KHCO_3$ did not significantly impact the conductivity and viscosity of NOHM-C-HPE while the viscosity and conductivity of NOHM-I-HPE decreased significantly as salt ions competed with the ionically tethered polymers to interact with the surface sites of the nanoparticle. Overall, the results presented here depict that the bond type and grafting density of NOHMs can be strategically selected to achieve the desired performance characteristics

for a variety of applications including DAC, CO_2 capture integrated with CO_2 conversion and/or redox flow batteries.

4. Experimental Section

4.1 Synthesis of NOHM-I-HPE. NOHM-I-HPE was synthesized at two grafting densities using a protocol very similar to our previously reported method.[31,34,36,37,44,45,82,83] A 30 wt.% colloidal suspension of 10 nm diameter SiO_2 nanoparticles (LUDOX SM-30 obtained from Sigma-Aldrich) was diluted to a concentration of 4 wt.% in deionized water. A 35 wt.% solution of the ionic linker, 3-(trihydroxysilyl)-1-propane-sulfonic acid (Gelest Inc.), was further diluted to a final concentration of 1 wt.% and was subsequently added to the SiO_2 nanoparticle solution in a dropwise manner. The ionic linker (referred to as SIT) was added so that the resulting surface coverage would be approximately 1.0 or 2.0 chains/nm^2. Then, 1 M NaOH was added dropwise to this solution until a pH of 5 was achieved and the final solution was stirred at 70 °C for 24 hrs. To protonate the sulfonate groups on the linker molecules and remove any other cations, the ionically functionalized silica nanoparticles were then passed through a cation-exchange resin (Dowex Marathon C hydrogen form, Sigma Aldrich). Next, an amine-terminated polyether, Jeffamine M2070 (MW=2000 g/mol, acquired from Huntsman Co.), was diluted to a concentration of 20 wt.% and ionically tethered to the functionalized nanoparticles. The Jeffamine M2070 polymer (referred to as HPE) was added dropwise in quantities so that the resulting grafting density would be approximately 1.0 or 2.0 chains/nm^2, prior to sample purification. Afterwards, the resulting aqueous suspension was left to mix overnight at room temperature. Any untethered polymers were then removed by dialyzing the solution against deionized water for at least 48 hr (SnakeSkin Dialysis Tubing 10K MW cutoff, Thermo Scientific), with frequent water changing (at least 8 times during the dialysis procedure). After dialysis, the aqueous solution of NOHMs was dried overnight in a vacuum oven at 60 ºC. It should be noted that after the dialysis process, it is possible that some linker sites may be unoccupied, as HPE chains that were not successfully tethered were washed out. The structure of NOHM-I-HPE can be observed in **Figure 1A**.

4.2 Synthesis of NOHM-C-HPE. Using a procedure similar to our previous studies,[31–33] NOHM-C-HPE was also synthesized at two different grafting densities. Briefly, HPE was dissolved in ethanol to a concentration of 3 wt.%. As with the ionic NOHMs, the amount of HPE polymer was selected so that the resulting grafting density would be approximately 1.0 or 2.0 chains/nm^2, prior to sample purification. Next, a molar equivalence of (3-glycidyloxypropyl) trimethoxysilane (acquired from Gelest Inc. and referred to as GPC) was diluted in ethanol to a concentration of about 3 wt.% and this mixture was added dropwise to the ethanol solution containing HPE. The resulting mixture was stirred for 12 hrs at 50 °C to ensure a complete reaction of the HPE chains with the GPC linker. After the reaction of the HPE polymer and the GPC linker was complete, the ethanol was removed via a typical distillation procedure, producing the GPC-functionalized HPE polymer. This functionalized HPE was then collected and diluted to a concentration of 7 wt.% (in deionized water) before being added dropwise to a 3 wt.% solution of SiO_2 nanoparticles (LUDOX SM-30 obtained from Sigma-Aldrich). The same overnight mixing, 48 hr dialysis process and water evaporation procedure (as described in the previous section) was also applied to the covalent NOHMs. The structure of NOHM-C-HPE is depicted in **Figure 1B**.

4.3 Differential scanning calorimetry (DSC). A DSC 200 F3 apparatus (NETZSCH), equipped with a liquid nitrogen Dewar, was employed to study the non-isothermal crystallization and melting behaviors of HPE, NOHM-I-HPE and NOHM-C-HPE. Briefly, the temperature was

scanned from 25 ºC to 100 ºC at a scan rate of 10 ºC/min, then the temperature was held isothermally at 100 ºC for a period of 5 minutes to erase thermal history. Afterwards, the temperature was cooled to -100 °C at a rate of 2.5 ºC/min and then subsequently heated to 100 ºC at a rate of 2.5 ºC/min. DSC experiments were performed at 2.5 ºC/min, instead of the commonly employed 10 ºC/min, to more closely observe the crystallization behaviors of the NOHMs. During all DSC measurements, the sample headspace was purged with Ar at a flowrate of 40 mL/min. About 15 mg of sample was loaded into an aluminum pan which was subsequently sealed and pierced. This process was repeated 3 times for each sample. The crystallinity (χ_c) of the HPE, NOHM-I-HPE and NOHM-C-HPE samples was determined using the following equation

$$\chi_c(\%) = \frac{\Delta H_m}{\Delta H_m^0} \times 100\% \qquad \textbf{Eq. (5)}$$

where ΔH_m is the melting enthalpy normalized by the weight of the polymer chains and ΔH_m^0 is the melting enthalpy of a 100% crystalline polyethylene oxide (PEO) with a value of 205 J/g.[57–59] Because of the presence of the SiO_2 nanoparticle in NOHMs, the polymer crystallinity in NOHM-I-HPE and NOHM-C-HPE samples was determined by accounting for only the mass of HPE present in NOHMs. It should also be noted that the HPE polymer in this study is a diblock copolymer which contains both polyethylene oxide (PEO) and polypropylene oxide (PPO) groups (See **Figure 1**), though it contains a majority of PEO groups. Thus, we assumed the enthalpy of melting of a perfectly crystalline PEO polymer (205 J/g)[57–59] to calculate the percent crystallinity in the HPE, NOHM-I-HPE and NOHM-C-HPE samples.

4.4 Non-isothermal Thermogravimetric Analysis (TGA). Thermogravimetric decomposition curves of HPE, NOHM-I-HPE and NOHM-C-HPE were collected in nitrogen and air atmospheres using a LabSys Evo (Setaram) TGA-DSC instrument. Prior to any TGA runs, samples were placed in a vacuum oven at 80 ºC for at least two hrs to remove any absorbed moisture. The heating program was set to run from 25 to 600 ºC, at a heating rate of 10 ºC/min. Between 5 and 10 mg of HPE, NOHM-I-HPE or NOHM-C-HPE was loaded into alumina crucibles and the gas (nitrogen or air) flowrate was set to 40 mL/min. Three trials were collected for each sample.

The mass percentage of SiO_2 nanoparticles in NOHMs was calculated based on the final mass of the sample at the end of each TGA run in nitrogen atmosphere, since the mass loss of NOHMs was due to the thermal decomposition of the organic components (*i.e.,* the HPE polymer and linker). **Table 3** outlines the final mass fraction of SiO_2 in each NOHMs sample, the approximate amounts of linker and polymer in each NOHMs sample and the corresponding grafting density of each NOHMs sample using the SiO_2 surface area provided by the manufacturer (Sigma Aldrich). Each NOHMs sample was labeled with its grafting density. For example, NOHM-I-HPE 0.4 refers to NOHM-I-HPE with a grafting density of 0.4 chains/nm^2 (rounded from the estimated value given in **Table 3**). It should be noted that because the reaction of the HPE with the nanoparticle surface was difficult to precisely control, the exact grafting densities we achieved for the final NOHM-I-HPE and NOHM-C-HPE samples were slightly different.

Table 3. Mass fractions of SiO_2, HPE and linker, as well as estimated grafting density for all NOHMs samples synthesized in this study[a]

	NOHM-I-HPE 0.4	***NOHM-I-HPE 0.8***	***NOHM-C-HPE 0.5***	***NOHM-C-HPE 0.7***
SiO_2 Mass Fraction	0.62	0.46	0.57	0.51
HPE Mass Fraction	0.31	0.47	0.40	0.45
Linker Mass Fraction	0.07	0.07	0.03	0.04
Estimated Grafting Density (chains/nm^2)	0.42	0.80	0.52	0.66
Physical appearance	Solid film/flakes	Gel-like	Solid film/flakes	Solid film/flakes

[a]The amount of HPE polymer, linker (ionic or covalent) and SiO_2 in each sample was estimated from the average of 3 TGA decomposition scans. The final grafting densities (chains/nm^2) of the prepared NOHMs samples were estimated using these values and the specific surface area of the SiO_2 nanoparticles provided by the manufacturer (Sigma Aldrich, 400 m^2/g).

4.5 Dynamic Light Scattering. The hydrodynamic diameters of the SiO_2 nanoparticles (d_{NP}), HPE (d_P), NOHM-I-HPE ($d_{NOHMs-I}$) and NOHM-C-HPE ($d_{NOHMs-C}$) in deionized water were measured using a dynamic light scattering (DLS) instrument (Zetasizer Nano ZS, Malvern Panalytical) at 25 °C. All samples were tested at a concentration of 0.1 wt.% to minimize the effects of multiple scattering, and the average of five measurements is reported for each sample. All samples were measured in disposable 2.5 mL plastic cuvettes (Brand) with a path length of 10 mm. Before being loaded into the cuvettes, the samples were passed through a syringe filter (Thermo Scientific) with a 0.2 μm pore size to remove any particulate impurities. The DLS experiments were performed at a 173° backscattering angle (NIBS default).

4.6 Small Angle Neutron Scattering. The samples used in small angle neutron scattering (SANS) measurements were prepared by dissolving NOHM-I-HPE 0.8 and NOHM-C-HPE 0.7 in deuterium oxide (D_2O) obtained from Sigma Aldrich. All the SANS experiments were performed at the high flux isotope reactor (HFIR) at the Oak Ridge National Laboratory on the CG-2 GP SANS beamline using three detector distances of 19 m, 5 m and 1 m to give a scattering vector, *Q,* range of 0.001−0.8 Å, at a wavelength of 4.75Å. The scattering vector, *Q*, can be represented by

$$Q = \frac{4\pi}{\lambda}\sin(\theta) \qquad \textbf{Eq. (6)}$$

where λ is the neutron wavelength and θ is the scattering angle. Samples were placed in 1 mm or 2 mm thick banjo cells. The measured scattering profiles of the samples were reduced using a reduction protocol written by the instrument scientist to correct for the thickness of the cell, empty cell scattering, sample transmission, and solvent scattering. The coherent scattering was fit and analyzed using SasView software, version 4.2.2.[84]

4.7 Viscosity measurement. The viscosity of SiO_2, HPE and NOHM-based fluids, with and without salt (0.1 M $KHCO_3$), were measured using a VISCOlab 4000 (Cambridge Viscosity – PAC) viscometer, which can measure viscosities from 0.2 to 10,000 cP. The temperature of the viscometer was maintained at 25.00 ± 0.05 °C using a water bath (VWR 1166D). The uncertainty in viscosity was determined to be within ± 5% for all samples.

4.8 Conductivity measurement. The ionic conductivities of the SiO_2, HPE and NOHM-based fluids, with and without salt (0.1 M $KHCO_3$), were measured at 25 ± 1 °C using an S230 SevenCompact benchtop conductivity meter (Mettler Toledo) equipped with a micro 2 platinum poles conductivity probe (Cond probe InLab 752 – 6mm, Mettler Toledo), which can measure conductivities in the range of 0.01 – 112 ms/cm. The uncertainty in conductivity was determined to be within ± 5% for all samples.

4.9 Attenuated Total Reflectance (ATR) FT-IR Spectroscopy. ATR FT-IR spectra were collected at room temperature (~ 25 ºC) using a Nicolet 6700 spectrometer equipped with a SurveyIR attachment (Czitek Ltd.) to chemically characterize the prepared NOHMs. The FT-IR spectra were recorded within a range of 600 – 4000 cm^{-1} using a resolution of 4 cm^{-1}. A total of 128 scans were recorded for each sample.

4.10 ^{1}H and ^{13}C NMR measurements. ^{1}H and ^{13}C NMR spectra of HPE, NOHM-I-HPE and NOHM-C-HPE were collected on a Bruker 400 AVIII. The samples were dissolved in D_2O to a concentration of about 10 mg/mL of HPE. All samples were mixed on a stir plate for at least 2 hrs. 540 µL of the dissolved sample was combined with 60 µL of a 2.0 M dimethylsulfone (internal standard) solution in an NMR tube. All samples were sonicated for at least 30 minutes before measurement. The NMR probe was tuned and shimmed. ^{1}H measurements were conducted with a recycle delay (d1) of 5 s and an acquisition time (AQ) of 6 s. A total of 16 scans and 4 dummy scans were collected for each sample, at 25 °C. ^{13}C measurements were conducted with a recycle delay (d1) of 1 s and an acquisition time (AQ) of 1 s. A total of 960 scans and 4 dummy scans were collected for each sample, at 25 °C.

Acknowledgements

This work was supported as part of the Breakthrough Electrolytes for Energy Storage (BEES), an Energy Frontier Research Center funded by the U.S. Department of Energy, Office of Science, Basic Energy Sciences under Award # DE-SC0019409 (exploration of bond type on the transport properties and structure of NOHMs in solution). The authors would also like to acknowledge Shell's Long Range Research and Experimentation (LRRE) Program for providing the funding for the part of this study focused on the characterization of the thermal stability of NOHM-I-HPE and NOHM-C-HPE. We would like to acknowledge LRRE's Dense Energy Carriers team (DEC) for their useful input and discussions during the course of this work. We also appreciate the Kumar group at Columbia University for allowing us to use their DLS instrument. Finally, the authors would like to acknowledge resources used during the SANS experiments at the High Flux Isotope Reactor, which is a DOE office of Science User Facility operated by the Oak Ridge National Laboratory.

Nomenclature

Variable	Definition
t	Time
T	Temperature
χ_c	Polymer percent crystallinity (%)
ΔH_m	Enthalpy of melting (J g^{-1})
ΔH_m^0	Enthalpy of melting of 100% crystalline polymer (J g^{-1})
ΔH_c	Enthalpy of crystallization (J g^{-1})
T_g	Glass transition temperature (°C)
T_c	Crystallization temperature (°C)
T_m	Melt temperature (°C)
$T_{10\%}$	Temperature at which 10% of the initial organic content has been degraded in a non-isothermal TGA experiment (°C)
$\Delta T_{10\%}$ (N_2 - Air)	The difference between the $T_{10\%}$ in nitrogen and the $T_{10\%}$ in air atmospheres (°C)
α	Extent of conversion
w_i	Initial weight fraction of sample subject to dynamic TGA scan
w	Weight fraction of sample subject to dynamic TGA scan at t or T
w_f	Final weight fraction of sample subject to dynamic TGA scan
d_P	Hydrodynamic diameter of HPE (nm)
d_{NOHMs}	Hydrodynamic diameter of NOHMs (nm)
d_{NP}	Hydrodynamic diameter of bare SiO_2 nanoparticles (nm)
d_N	Thickness of polymer layer in NOHMs (nm)
Q	Scattering vector
λ	Neutron wavelength
θ	Scattering angle
$I(Q)$	Scattering intensity
η	Viscosity (cP)
η_s	Viscosity of solvent (cP)
η_{sp}	Specific viscosity
c	Concentration (g mL^{-1})
$\Delta\eta$	Percent viscosity difference upon salt addition (%)
η_{SE}	Viscosity of electrolyte (cP)
κ	Ionic conductivity (mS cm^{-1})

References

[1] M. Alves, R. Segurado, M. Costa, *Energy* **2020**, *198*, 117321.
[2] L. Liu, Z. Wang, Y. Wang, J. Wang, R. Chang, G. He, W. Tang, Z. Gao, J. Li, C. Liu, L. Zhao, D. Qin, S. Li, *Renew. Sustain. Energy Rev.* **2020**, *132*, 110151.
[3] B. Gurkan, H. Squire, E. Pentzer, *J. Phys. Chem. Lett.* **2019**, *10*, 7956.
[4] Y. Chen, T. Mu, *Green Chem.* **2019**, *21*, 2544.
[5] H. K. Lim, H. Kim, *Molecules* **2017**, *22*, 536.
[6] M. H. Chakrabarti, F. S. Mjalli, I. M. Alnashef, M. A. Hashim, M. A. Hussain, L. Bahadori, C. T. J. Low, *Renew. Sustain. Energy Rev.* **2014**, *30*, 254.
[7] C. V. Amanchukwu, *Joule* **2020**, *4*, 281.
[8] Y. Y. Lai, X. Li, Y. Zhu, *ACS Appl. Polym. Mater.* **2020**, *2*, 113.
[9] N. M. Cantillo, M. Bruce, S. T. Hamilton, T. G. Feric, A.-H. A. Park, T. Zawodzinski, *J. Electrochem. Soc.* **2020**, *167*, 116508.
[10] S. Overa, T. G. Feric, A.-H. A. Park, F. Jiao, *Joule* **2021**, *5*, 8.
[11] M. Konig, J. Vaes, E. Klemm, D. Pant, *iScience* **2019**, *19*, 135.
[12] M. Dunwell, X. Yang, B. P. Setzler, J. Anibal, Y. Yan, B. Xu, *ACS Catal.* **2018**, *8*, 3999.
[13] S. Nitopi, E. Bertheussen, S. B. Scott, X. Liu, A. K. Engstfeld, S. Horch, B. Seger, I. E. L. Stephens, K. Chan, C. Hahn, J. K. Nørskov, T. F. Jaramillo, Chorkendor, *Chem. Rev.* **2019**, *119*, 7610.
[14] G. L. Soloveichik, *Chem. Rev.* **2015**, *115*, 11533.
[15] X. Wei, W. Pan, W. Duan, A. Hollas, Z. Yang, B. Li, Z. Nie, J. Liu, D. Reed, W. Wang, V. Sprenkle, *ACS Energy Lett.* **2017**, *2*, 2187.
[16] L. Sun, G. K. Ramesha, P. V. Kamat, J. F. Brennecke, *Langmuir* **2014**, *30*, 6302.
[17] M. Heres, T. Cosby, E. U. Mapesa, H. Liu, S. Berdzinski, V. Strehmel, M. Dadmun, S. J. Paddison, J. Sangoro, *Macromolecules* **2019**, *52*, 88.
[18] D. Shen, K. Steinberg, R. Akolkar, *J. Electrochem. Soc.* **2018**, *165*, E808.
[19] D. V. Vasilyev, A. V. Rudnev, P. Broekmann, P. J. Dyson, *ChemSusChem* **2019**, *12*, 1635.
[20] S. Verma, X. Lu, S. Ma, R. I. Masel, P. J. A. Kenis, *Phys. Chem. Chem. Phys.* **2016**, *18*, 7075.
[21] B. B. Hansen, S. Spittle, B. Chen, D. Poe, Y. Zhang, J. M. Klein, A. Horton, L. Adhikari, T. Zelovich, B. W. Doherty, B. Gurkan, E. J. Maginn, A. Ragauskas, M. Dadmun, T. A. Zawodzinski, G. A. Baker, M. E. Tuckerman, R. F. Savinell, J. R. Sangoro, *Chem. Rev.* **2021**, *121*, 1232.
[22] L. Chang, A. J. Bard, *J. Electrochem. Soc.* **2020**, *167*, 066505.
[23] J. Peng, N. M. Cantillo, K. M. K. Nelms, L. S. Roberts, G. Goenaga, A. Imel, B. A. Barth, M. Dadmun, L. Heroux, D. G. Hayes, T. Zawodzinski, *ACS Appl. Mater. Interfaces* **2020**, *12*, 40213.
[24] X. Shen, N. Sinclair, J. Wainright, A. Imel, B. Barth, T. Zawodzinski, R. F. Savinell, *J. Electrochem. Soc.* **2021**, *168*, 060539.
[25] J. Peng, Y. Xiao, A. Imel, B. A. Barth, N. M. Cantillo, K. M. K. Nelms, T. A. Zawodzinski, *Electrochim. Acta* **2021**, *393*, 139048.
[26] J. Peng, N. M. Cantillo, Y. Xiao, K. M. Nelms, L. S. Roberts, G. Goenaga, A. Imel, B. A. Barth, M. Dadmun, D. G. Hayes, T. Zawodzinski, *J. Electrochem. Soc.* **2021**, *168*, 080502.

[27] S. Srivastava, S. Choudhury, A. Agrawal, L. A. Archer, *Curr. Opin. Chem. Eng.* **2017**, *16*, 92.
[28] W. Yu, T. Wang, A.-H. A. Park, M. Fang, *Nanoscale* **2019**, *11*, 17137.
[29] S. Choudhury, A. Agrawal, S. Wei, E. Jeng, L. A. Archer, *Chem. Mater.* **2016**, *28*, 2147.
[30] A. Agrawal, S. Choudhury, L. A. Archer, *RSC Adv.* **2015**, *5*, 20800.
[31] C. Petit, S. Bhatnagar, A.-H. A. Park, *J. Colloid Interface Sci.* **2013**, *407*, 102.
[32] K.-Y. A. Lin, C. Petit, A.-H. A. Park, *Energy & Fuels* **2013**, *27*, 4167.
[33] K.-Y. A. Lin, A.-H. A. Park, *Environ. Sci. Technol.* **2011**, *45*, 6633.
[34] T. G. Feric, S. T. Hamilton, N. M. Cantillo, A. E. Imel, T. A. Zawodzinski, A.-H. A. Park, *J. Phys. Chem. B* **2021**, *125*, 9223.
[35] M. D. Dadmun, M. A. Haque, T. G. Feric, S. T. Hamilton, A.-H. A. Park, *J. Phys. Chem. C* **2021**, *125*, 5327.
[36] S. Moon, Y. Lee, S. Choi, S. Hong, S. Lee, A.-H. A. Park, Y. Park, *Org. Process Res. Dev.* **2018**, *22*, 1723.
[37] S. Choi, S. Moon, Y. Park, *Langmuir* **2020**, *36*, 9626.
[38] E. U. Mapesa, N. M. Cantillo, S. T. Hamilton, M. A. Harris, T. A. Zawodzinski, A. A. Park, J. Sangoro, *Macromolecules* **2021**, *54*, 2296.
[39] K.-Y. A. Lin, Y. Park, C. Petit, A.-H. A. Park, *RSC Adv.* **2014**, *4*, 65195.
[40] C. Petit, K.-Y. A. Lin, A.-H. A. Park, *Langmuir* **2013**, *29*, 12234.
[41] T. G. Feric, S. T. Hamilton, A. H. A. Park, *Energy and Fuels* **2021**, *35*, 19592.
[42] G. Rim, T. G. Feric, T. Moore, A.-H. A. Park, *Adv. Funct. Mater.* **2021**, *31*, 1.
[43] J. L. Schaefer, S. S. Moganty, D. A. Yanga, L. A. Archer, *J. Mater. Chem.* **2011**, *21*, 10094.
[44] Y. Park, J. Decatur, K.-Y. A. Lin, A.-H. A. Park, *Phys. Chem. Chem. Phys.* **2011**, *13*, 18115.
[45] C. Petit, Y. Park, K.-Y. A. Lin, A.-H. A. Park, *J. Phys. Chem. C* **2012**, *116*, 516.
[46] Y. Park, C. Petit, P. Han, A.-H. A. Park, *RSC Adv.* **2014**, *4*, 8723.
[47] Y. Park, D. Shin, Y. N. Jang, A.-H. A. Park, *J. Chem. Eng. Data* **2012**, *57*, 40.
[48] Y. Park, K.-Y. A. Lin, A.-H. A. Park, C. Petit, *Front. Energy Res.* **2015**, *3*, 1.
[49] K.-Y. A. Lin, H. Yang, W.-D. Der Lee, K.-Y. Y. Tsao, *J. Mol. Liq.* **2015**, *204*, 50.
[50] S. T. Hamilton, T. G. Feric, G. Andrzej, N. M. Cantillo, T. A. Zawodzinski, A. A. Park, *ACS Appl. Mater. Interfaces* **2022**, *14*, 22016.
[51] S. T. Hamilton, T. G. Feric, S. Bhattacharyya, N. M. Cantillo, S. G. Greenbaum, T. A. Zawodzinski, A.-H. A. Park, *J. Am. Chem. Soc. Au* **2022**.
[52] Y. Zhang, D. Poe, L. Heroux, H. Squire, B. W. Doherty, Z. Long, M. Dadmun, B. Gurkan, M. E. Tuckerman, E. J. Maginn, *J. Phys. Chem. B* **2020**, *124*, 5251.
[53] J. M. Klein, H. Squire, W. Dean, B. E. Gurkan, *J. Phys. Chem. B* **2020**, *124*, 6348.
[54] N. K. Jayakody, C. C. Fraenza, S. G. Greenbaum, D. Ashby, B. S. Dunn, *J. Phys. Chem. B* **2020**, *124*, 6843.
[55] S. Liu, M. Walton, N. V. Tarakina, P. Akcora, *J. Phys. Chem. B* **2020**, *124*, 4843.
[56] J. M. Klein, H. Squire, B. Gurkan, *J. Phys. Chem. C* **2020**, *124*, 5613.
[57] X. Wen, Y. Su, Y. Shui, W. Zhao, A. J. Müller, D. Wang, *Macromolecules* **2019**, *52*, 1505.
[58] W. Zhao, Y. Su, X. Gao, J. Xu, D. Wang, *J. Polym. Sci. Part B Polym. Phys.* **2016**, *54*, 414.
[59] L. Zhao, W. Kai, Y. He, B. Zhu, Y. Inoue, *J. Polym. Sci. Part B Polym. Phys.* **2005**, *43*,

2665.
[60] Y. Meng, J. Jiang, A. Aihemaiti, T. Ju, Y. Gao, J. Liu, S. Han, *ACS Appl. Mater. Interfaces* **2019**, *11*, 33781.
[61] C. J. Yoo, S. J. Park, C. W. Jones, *Ind. Eng. Chem. Res.* **2020**, *59*, 7061.
[62] S. H. Pang, L. C. Lee, M. A. Sakwa-Novak, R. P. Lively, C. W. Jones, *J. Am. Chem. Soc.* **2017**, *139*, 3627.
[63] S. H. Pang, R. P. Lively, C. W. Jones, *ChemSusChem* **2018**, *11*, 2628.
[64] A. Ahmadalinezhad, A. Sayari, *Phys. Chem. Chem. Phys.* **2014**, *16*, 1529.
[65] Y. Shui, Y. Su, X. Kuang, W. Zhao, Y. Cai, D. Wang, *Polym. Int.* **2017**, *66*, 1395.
[66] K. Chrissafis, D. Bikiaris, *Thermochim. Acta* **2011**, *523*, 1.
[67] R. Heidar Pour, M. Soheilmoghaddam, A. Hassan, S. Bourbigot, *Polym. Degrad. Stab.* **2015**, *120*, 88.
[68] A. Chamas, H. Moon, J. Zheng, Y. Qiu, T. Tabassum, J. H. Jang, M. Abu-Omar, S. L. Scott, S. Suh, *ACS Sustain. Chem. Eng.* **2020**, *8*, 3494.
[69] P. Navarro, M. Larriba, E. Rojo, J. García, F. Rodríguez, *J. Chem. Eng. Data* **2013**, *58*, 2187.
[70] R. Balart, D. Garcia-Sanoguera, L. Quiles-Carrillo, N. Montanes, S. Torres-Giner, *Polymers (Basel).* **2019**, *11*, 281.
[71] M. L. Williams, J. S. Dickmann, M. E. McCorkill, J. C. Hassler, E. Kiran, *Thermochim. Acta* **2020**, *685*, 25.
[72] S. McDonald, J. A. Wood, P. A. FitzGerald, V. S. J. Craig, G. G. Warr, R. Atkin, *Langmuir* **2015**, *31*, 3763.
[73] A. Guinier, G. Fournet, C. B. Walker, *SCATTERING OF X-RAYS*, John Wiley & Sons, New York, **1955**.
[74] H. Jonassen, A. L. Kjøniksen, M. Hiorth, *Colloid Polym. Sci.* **2012**, *290*, 919.
[75] S. Jailani, G. V. Franks, T. W. Healy, *J. Am. Ceram. Soc.* **2008**, *91*, 1141.
[76] B. Lego, W. G. Skene, S. Giasson, *Macromolecules* **2010**, *43*, 4384.
[77] R. Ortiz, S. Olsen, E. Thormann, *Langmuir* **2018**, *34*, 4455.
[78] I. M. Mahbubul, R. Saidur, M. A. Amalina, *Int. J. Heat Mass Transf.* **2012**, *55*, 874.
[79] S. O. Olayiwola, M. Dejam, *Ind. Eng. Chem. Res.* **2020**, *59*, 3575.
[80] L. Poudel, R. Podgornik, W. Y. Ching, *J. Phys. Chem. A* **2017**, *121*, 4721.
[81] Y. Inokuchi, T. Ebata, T. Ikeda, T. Haino, T. Kimura, H. Guo, Y. Furutani, *New J. Chem.* **2015**, *39*, 8673.
[82] K.-Y. A. Lin, C. Petit, A.-H. A. Park, *Energy & Fuels* **2013**, *27*, 4167.
[83] Y. Park, D. Shin, Y. N. Jang, A.-H. A. H. A. Park, *J. Chem. Eng. Data* **2012**, *57*, 40.
[84] SasView - Small Angle Scattering Analysis.